Available online at www.sciencedirect.com
SCIENCE DIRECT®
Nuclear Instruments and Methods in Physics Research B 249 (2006) 114–117
NIM B
Beam Interactions with Materials & Atoms
www.elsevier.com/locate/nimb

GISAXS studies of structural modifications in ion-beam amorphized Ge

I.D. Desnica-Franković [a,*], P. Dubcek [a], U.V. Desnica [a], S. Bernstorff [b], M.C. Ridgway [c], C.J. Glover [c]

[a] R. Boskovic Institute, Materials Physics Division, P.O. Box 180, 10002 Zagreb, Croatia
[b] Sincrotrone Trieste, SS 14 km163,5, 34012 Basovizza, Italy
[c] Department of Electronic Materials Engineering, Australian National University, Canberra, Australia

Available online 11 May 2006

Abstract

Grazing incidence small angle scattering of X-rays (GISAXS) was used to analyze structural modifications in implantation-damaged Ge. Samples were implanted by different doses of ^{74}Ge, from 3×10^{12} cm^{-2} to 3×10^{16} cm^{-2}; at room- or liquid nitrogen-temperature, respectively. We have found that the micro-structure in amorphous Ge, continuously and consistently evolves as a function of ion dose but differs according to the implantation temperature. In RT-samples small vacancy nanoclusters agglomerate in the end-of-range region of implanted layer even before complete amorphization. With higher doses nanoclusters increase and coalesce into nano-voids. For the highest dose, the onset of porosity is confirmed. On the other hand, in LN-implanted samples, the clustering-related signal is much weaker and evolves more slowly.

PACS: 61.10.Eq; 61.43.–j; 61.43.Dq; 61.72.Ji

Keywords: Amorphous Ge; Ion implantation; GISAXS; Nano-voids; Porosity

1. Introduction

Implantation induced disorder is of great interest for both basic understanding and technological applications, since ion beam processing is a powerful and versatile tool in many areas of technology. However, the amount of inhomogeneities, concentration fluctuations and nano- and micro-voids, and finally the ultimate properties of the processed material strongly depend on the implantation parameters and post-implantation treatments [1–3]. Thus, for the establishment or enhancement of some specific characteristics (like porosity or void-less structure, or micro-, nano-crystallinity) the appropriate values for the processing parameters have to be chosen. A specific goal of this study is to assist in establishing the proper implantation–parameter semiconductor–structure correlation.

Experimentally, amorphous semiconductors always show a density deficit relative to the crystalline material [4]. The possible explanation is a small increase in average bond length or the presence of a small density of nm-sized voids. EXAFS measurements revealed an increase in the nearest neighbor distance in Ge on the crystalline- to amorphous-phase transition, as well as an increase in bond length and structural disorder with ion dose [5,6]. Since the increased dose produces an increased number of Frankel pairs, the increased number of vacancies and interstitials should lead to a net lattice expansion. Porosity has currently attracted a renewed interest after the discovery of light emitting properties of porous silicon but comparatively little work has been carried out on Ge [7].

GISAXS, which is sensitive to electron density fluctuations, may expose the existence of nano-voids in the

* Corresponding author. Tel.: +385 1468 0988; fax: +385 1468 0114.
E-mail address: ddesnica@rudjer.irb.hr (I.D. Desnica-Franković).

0168-583X/$ - see front matter © 2006 Elsevier B.V. All rights reserved.
doi:10.1016/j.nimb.2006.03.093

material and provide a means to establish the concentration, sizes and size distribution of voids in thin amorphous layers. It could be an ideal tool to resolve the important question of implantation induced microstructural modifications in a-Ge, and the question whether the void-less amorphous material can be prepared by self-implantation.

2. Experimental procedure

A 2 μm thick, MBE grown monocrystalline Ge samples were implanted with 500 keV ^{74}Ge ions. The applied doses were ranging from 3×10^{12} to 3×10^{16} cm^{-2}, implantation was done at either 21 °C or at LN-temperature (−196 °C). A low ion flux (power density ~ 0.5 W/cm^2) was utilized to avoid beam induced heating during implantation. After implantation, the samples were characterized by Rutherford back-scattering (RBS) and then analyzed by Raman scattering [8]. Analogous set of samples, prepared under the same implantation conditions, has been analyzed by extended X-ray fine-structure spectroscopy (EXAFS) [6,9].

Grazing incidence small angle X-ray scattering (GISAXS) measurements were performed at the synchrotron ELETTRA, Trieste (Italy), at the SAXS beamline [10] using the X-ray beam energy 8 keV ($\lambda = 0.154$ nm). GISAXS spectra were measured for seven grazing angles of incidence, starting with the critical angle for total external reflection ($\alpha_{C,Ge} = 0.32°$) and then subsequently increasing the angle in 0.05° steps. X-ray scattering intensity spectra were acquired by a two-dimensional position sensitive CCD detector at a detector to sample distance of $L = 2000$ mm. The quasi-particle related spectra were analyzed by Guinier approximation. The diameter of particles was determined from the 1D cut using the simple Guinier-plot analysis. The Guinier radius was calculated from the slope of the linear part of the ln $I(q)$ versus q^2 dependence, for $q > q_{max}$, ($q = (4\pi/\lambda)\sin\theta$; 2θ is the scattering angle). Prior to the analysis spectra were corrected for background intensity and detector response, and then for refraction and absorption effects.

3. Results and discussion

Since a very wide range of ion doses has been used (3×10^{12}–3×10^{16} cm^{-2}) this investigation covers several stages in the microstructural modifications. Selected 2D GISAXS spectra obtained on progressively higher-dose implanted samples are presented in Fig. 1. Left- and right-hand side panels represent samples implanted with same doses at RT- and LN-temperature, respectively. The topmost samples, implanted at 3×10^{13} cm^{-2} are damaged but still partly crystalline, rendering the weakest scattering related signal. All others are implanted at doses beyond the amorphization threshold and the evolution of microstructural modifications with dose is reflected in the systematic transformations in the scattering signal. For RT-samples implanted at low doses the scattered signal comes from

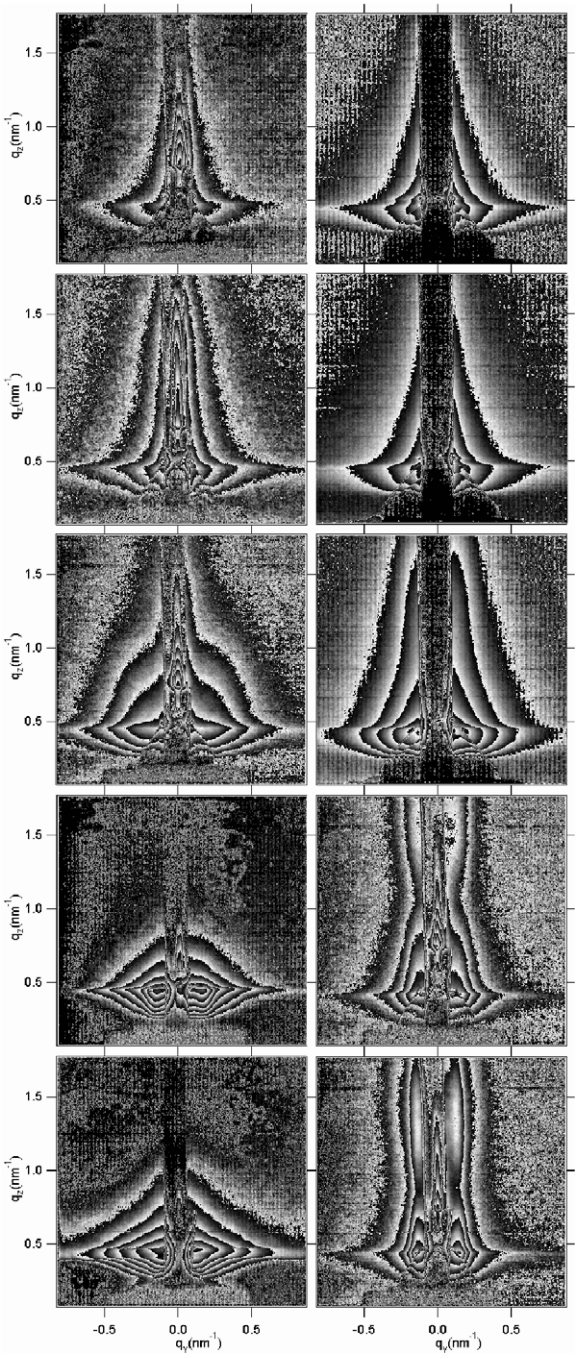

Fig. 1. A set of 2D GISAXS patterns taken on the Ge samples at the incidence angle $\alpha_i = \alpha_c + 0.1°$. The Al-foil vertical beam-stopper attenuates the specular-plane intensity. Samples were implanted at RT (left column) and LN-temperature (right) by successively increased doses of ^{74}Ge ions, the topmost samples implanted at 3×10^{13} cm^{-2}, following by 1×10^{14} cm^{-2}, 1×10^{15} cm^{-2}, 1×10^{16} cm^{-2}, and the last row implanted by 3×10^{16} cm^{-2}.

the damaged surface – rough surface SAXS signal. As the fluence is increased (1×10^{15} cm^{-2}) the particle-related ring-like signal appears – assigned to clustering of vacancies into nanometric sized agglomerates. Finally, the signal of the porous material is obtained for fluence 3×10^{16} cm^{-2}, consistent with the onset of porosity as found also by TEM [7]. Implantation-induced porosity

has been attributed to the nucleation and growth of void-like cavities via vacancy clustering. In LN-samples no porosity was observed whatsoever; however pronounced second order maxima in the vicinity of the specular plane for two highest doses indicate a correlated ensemble of flattened cylinder-like voids with very narrow size distribution arranged laterally in the implanted layer.

Fig. 2 depicts analysis of the intensity variation in the specular plane (left) and in off-specular vertical cut of the 2D image (right). For the 3×10^{13} cm^{-2} dose (top), a significant intensity variation accompanied with a pronounced hump for the largest grazing angles suggests scattering which is typical for the presence of nanoparticles distributed within the matrix. The absence of any particle related scattering in the off-specular cut indicates very broad size distribution (right). During the process of implantation a highly damaged layer is being formed in the end-of-range region. With increased dose this region is gradually amorphized and nucleation and grow of vacancy clustering starts, giving rise to a well defined hump even for the sample (3×10^{13} cm^{-2}) which is not yet completely amorphous. For the 3×10^{14} cm^{-2} dose the specular-plane signal is even more pronounced; a shoulder in the off-specular vertical cut is related to a system of laterally distributed platelet-shaped quasi-particles; with diameter 9 nm, height 5 nm, on average. For the comparison, an analogous 1D spectrum taken from the non-implanted samples is presented as well.

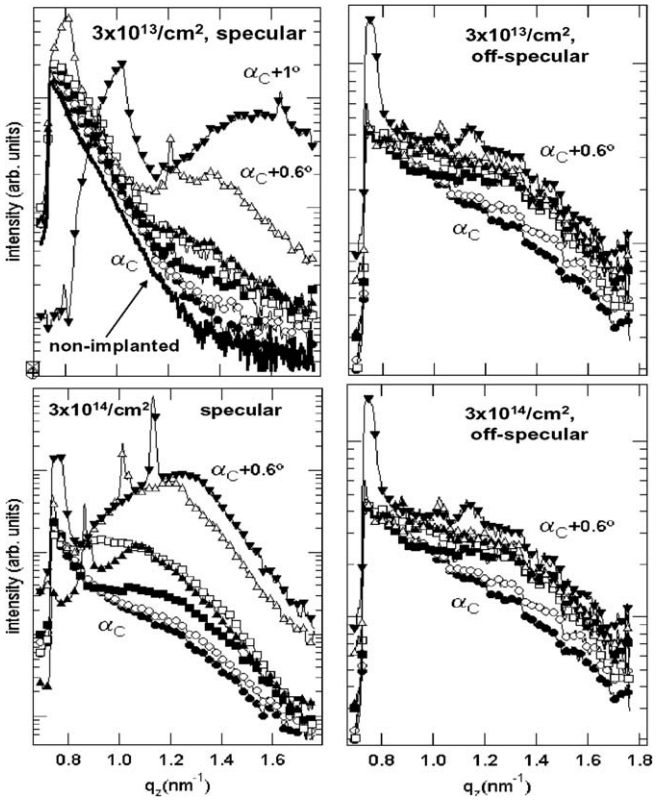

Fig. 2. 1D cross-sections of GISAXS patterns of Fig. 1 for the 3×10^{13} cm^{-2} (top) and 3×10^{14} cm^{-2} (bottom) RT-samples cut in the specular plane (left) and off-specular, parallel to q_z(right). The incidence angle has been increased from the critical angle α_C in 0.05°-steps. For comparison, an analogous 1D cut of the 2D spectrum taken from the non-implanted samples is presented as well.

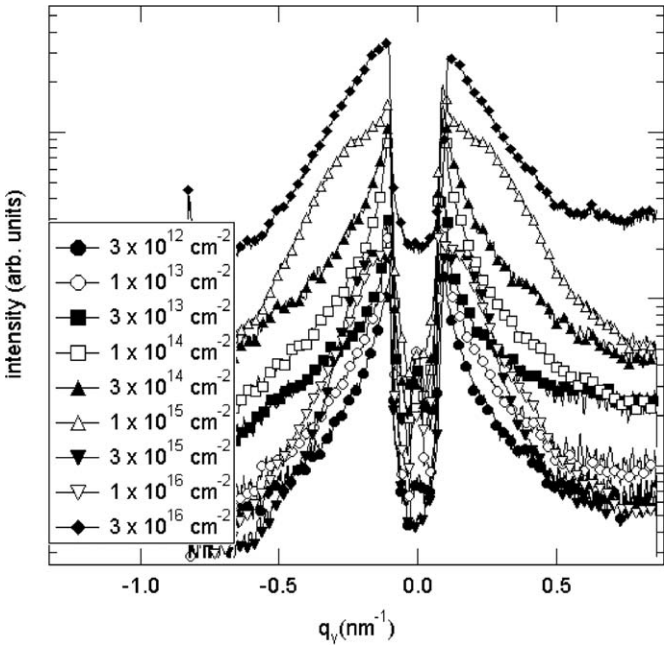

Fig. 3. A cross-section of the 2D GISAXS scattering patterns along direction parallel to the q_y axis for RT-implanted samples. Curves are shifted vertically for clarity.

Since GISAXS is sensitive to the change of electronic density, vacancy clustering into small voids should be readily observable as a characteristic, quasi-particle-related signal. The development and progression of the vacancy-clustering signal could be further followed in Fig. 3 which depicts 1D cross-section parallel to q_y for $\alpha_i = \alpha_{crit} + 0.1°$. The well defined flattened vacancy-agglomerates of 10.6 nm average size, could be resolved in the 1×10^{15} cm^{-2} – dose sample. In the 3×10^{15} cm^{-2} – dose sample nano-clusters become more spherical, and grow in size to 17 nm. For even higher doses nanoclusters agglomerate into large voids, of broad size distribution; it is an onset of porosity, which completely dominates in the 3×10^{16} cm^{-2} – dose sample implanted at RT. Thus, in RT-implanted samples the thermal energy, in addition to the energy supplied by implantation, has been sufficient to induce diffusion and restructuring of defects, clustering of vacancies into voids and finally the porosity.

4. Conclusions

We have used X-ray scattering of synchrotron radiation at grazing angles to investigate the morphology evolution in monocrystalline germanium damaged and amorphized by self-implantation with ^{74}Ge. We have found that the micro-structure in amorphous Ge, continuously and consistently evolves as a function of the ion dose, but the changes differ depending on implantation temperature. In RT-samples, changes in the GISAXS spectra correspond to the dose-dependant formation and expansion of highly

damaged sections. Even prior to the amorphization threshold the nucleation and growth of small vacancy-agglomerates begins deeper-in in the implanted layer. After the 1E15 cm^{-2} dose, a signal is interpreted as the start-up of vacancy clustering into larger voids. For further dose increase, this void-related signal becomes dominant and completely prevails after the 1E16 cm^{-2}-dose; the voids coalesce and the average void size is growing to the 17 nm range. For the 3E16 cm^{-2}-dose, quasi-particle related signal vanishes – the result supports the onset of porosity, which was observed previously with TEM [7]. On the other hand, in LN-implanted samples, the clustering-related signal is much weaker than the 'damage'-related one. Only for the highest doses laterally arranged correlated vacancy agglomerates form in the amorphous layer.

GISAXS has emerged as one of a very few methods sensitive to the nanometer-sized structural changes in amorphous material, giving an abundance of information and excellently complements other characterization methods.

Acknowledgements

The research has been supported by the Ministry of Science and Technology of the Republic of Croatia. M.C.R. and C.J.G. were supported by the Australia Synchrotron Research Program, funded by the Commonwealth of Australia.

References

[1] T.E. Haynes, O.W. Holland, Appl. Phys. Lett. 58 (1991) 452.
[2] S. Roorda, W.C. Sinke, J.M. Poate, D.C. Jacobson, S. Dierker, B.S. Dennis, D.J. Eaglesham, F. Spaepen, P. Fuoss, Phys. Rev. B 44 (1991) 3702.
[3] I.D. Desnica-Frankovic, J. Appl. Phys. 85 (1999) 7587, and references therein.
[4] D.L. Williamson, S. Roorda, M. Chicioine, R. Tabti, P.A. Stolk, S. Acco, F.W. Saris, Appl. Phys. Lett. 67 (1995) 226.
[5] M.C. Ridgway, J.C. Glover, I.D. Desnica-Frankovic, K. Furic, K.M. Yu, G.J. Foran, C. Clerc, J.L. Hansen, A. Nylandsted Larsen, Nucl. Instr. and Meth. B 175–177 (2001) 21.
[6] M.C. Ridgway, J.C. Glover, K.M. Yu, G.J. Foran, C. Clerc, J.L. Hansen, A. Nylandsted Larsen, Phys. Rev. B 61 (2000) 12586.
[7] L.M. Wang, R.C. Birtcher, Philos. Mag. A 64 (1991) 1209.
[8] I.D. Desnica-Frankovic, K. Furic, U.V. Desnica, M.C. Ridgway, C.J. Glover, Nucl. Instr. and Meth. B. 178 (2001) 192.
[9] J.C. Glover, M.C. Ridgway, K.M. Yu, G.J. Foran, D. Desnica-Frankovic, C. Clerc, J.L. Hansen, A. Nylandsted Larsen, Phys. Rev. B 63 (2001) 073204.
[10] H. Amenitsch, S. Bernstorff, M. Rappolt, Kriechbaum, H. Mio, P. Laggner, J. Synchrotron Rad. 5 (1998) 506.